Ortigosa, N.; Rodriguez-Lopez, M.; Bailón, R.; Sarvari, SI.; Sitges, M.; Gratacos, E.; Bijnens, B.... (2016). Heart morphology differences induced by intrauterine growth restriction and preterm birth measured on the ECG at preadolescent age. Journal of Electrocardiology. 49(3):401-409. doi:10.1016/j.jelectrocard.2016.03.011.

Heart morphology differences induced by intrauterine growth restriction and preterm birth measured on the ECG at preadolescent age

Nuria Ortigosa[a], Merida Rodriguez-Lopez[b], Raquel Bailón[c,d], Sebastian Imre Sarvari[e,f], Marta Sitges[e], Eduard Gratacos[b], Bart Bijnens[g], Fatima Crispi[b], Pablo Laguna[c,d]

[a] *I.U. Matemática Pura y aplicada, Universitat Politècnica de València Camino de Vera s/n, 46022 Valencia, Spain*
nuorar@upvnet.upv.es
[b] *Fetal i+D Medicine Research Center, BCNatal-Barcelona Center for Maternal-Fetal and Neonatal Medicine (Hospitals Clinic and Sant Joan de Deu). IDIBAPS, University of Barcelona (CIBER-ER)*
[c] *BSICoS Group, Aragón Institute of Engineering Research (I3A), IIS Aragón. University of Zaragoza, Spain*
[d] *Centro de Investigación Biomédica en Red en Bioingeniería, Biomateriales y Nanomedicina (CIBER-BBN), Spain*
[e] *Cardiovascular Institute, Hospital Clinic, IDIBAPS, University of Barcelona, Institut d'Investigacions Biomèdiques August Pi i Sunyer, Barcelona, Spain*
[f] *Department of Cardiology, Oslo University Hospital, Rikshospitalet, and University of Oslo, Norway.*
[g] *ICREA, Universitat Pompeu Fabra, Spain.*

Abstract

Intrauterine Growth Restriction (IUGR) and premature birth are associated with higher risk of cardiovascular diseases throughout adulthood. The aim of this study was to evaluate the influence of these factors in ventricular electrical remodeling in preadolescents. Electrocardiography was performed in a cohort of 33-IUGR, 32-preterm with appropriate weight and 60 controls. Depolarization and repolarization processes were studied by means of the surface ECG, including loops and angles corresponding to QRS and T-waves. The angles between the dominant vector of QRS and the frontal plane XY were different among the study groups: controls [20.03º(10.11º-28.64º)], preterm [25.48º(19.79º-33.56º)], and IUGR [27.77º(16.59º-33.23º)]. When compared to controls, IUGR subjects also presented wider angles between the difference of QRS and T-wave dominant vectors and the XY-plane [5.28º±12.15º

vs 0.49º±14.15º, p< 0.05] while preterm ones showed smaller frontal QRS-T angle [4.68º(2.20º-12.89º) vs 6.57º(2.72º-11.31º), p<0.05]. Thus, electrical remodeling is present in IUGR and preterm preadolescents, and might predispose them to cardiovascular diseases in adulthood. Follow-up studies are warranted.

Keywords: Premature birth, Intrauterine Growth Restriction, ventricular electrical remodelling

1. Introduction

For many years, genetics and lifestyle have been considered as the main cardiovascular risk factors. However, by the 90s, Barker and colleagues demonstrated a strong association between cardiovascular diseases (CVD) and birthweight [1], and proposed that low birthweight may produce structural and functional changes in key organs in postnatal life that predispose to CVD in adulthood, from which the concept of fetal programming emerged [1]. In this paper, we studied two leading causes of low birthweight: intrauterine growth restriction (IUGR) and preterm delivery.

IUGR affects 7-10% of pregnancies and is defined as the failure of a fetus to achieve its growth potential [2]. It is usually associated with placental insufficiency that determines fetal hypoxia, undernutrition and pressure/volume overload. Several studies have demonstrated that IUGR fetuses [3] and children with earlier IUGR [4] show significant changes in cardiac structure and function in the form of more spherical hearts with reduced longitudinal motion and impaired relaxation. On the other hand, prematurity represents 4-10% of deliveries and is defined by birth before 37 completed weeks of gestation. Preterm birth has multiple causes, including spontaneous preterm labor, intraamniotic inflammation and/or infection, preterm rupture of membranes, and labor induction due to IUGR or preeclampsia. Recently, increased cardiac mass together with short and small left ventricles have been described in adults born preterm [5].

In addition, both IUGR and prematurity have been associated with increased CVD in adulthood [6] as well as with arrhythmias i.e sudden death syndrome [7] and apnea-bradycardia episodes [8] in infants. However, little is known about the presence of electrical changes associated with these conditions that could predispose to long-term consequences. It has been proposed that electrical remodelling could occur primarily or secondary to the cardiac

structural remodelling described in these conditions [9].

Hence, the aim of the present study was to identify signs of ventricular electrical remodelling in preterm and growth restricted babies on reaching preadolescence by assessing changes in ventricular depolarization and repolarization using the QRS complex and T-wave, respectively. This was assessed by analyzing the direction of the QRS and T vectors, as well as the angle between them, which is supposed to reflect possible deviations between ventricular depolarization and repolarization. Finally, an analysis of QRS and T loop morphology was also performed in order to study in detail the presence of abnormalities in the ECG signal.

2. Materials and Methods

2.1. Study populations

The study population included 125 preadolescents, whose surface 12-lead ECG was recorded at a sampling rate of 1000 Hz in a tertiary center. 33 subjects had severe IUGR with medically-induced preterm delivery, 32 were spontaneously born preterm with appropriate weight for gestational age (AGA) and 60 normally grown controls born at term. From now on, these three groups will be denoted by preterm-IUGR, preterm-AGA and controls. IUGR was defined by low birthweight below 10th centile and abnormal umbilical artery Doppler (pulsatility index above the 95th centile), while adequate growth was considered if birthweight was above 10th centile for gestational age according to local standards [10]. Preterm birth was defined by delivery before 37 completed weeks of gestation. Gestational age was calculated by first-trimester crown-rump length measurement by ultrasound. Cases and controls were selected from a previously published cohort study that included 200 children at 2-6 years of age whose gestational age ranged from 25 to 41 weeks [4], which was conducted in a tertiary referral university hospital in Barcelona, Spain. We contacted all previous study participants to be included in this follow-up (6 years after the previous cardiovascular assessment) and 125 accepted to be recruited for the present study.

Digital standard 12-lead surface ECGs were recorded using a Gem Heart One recorder (Gem-Med SL, Spain), at an equivalent paper speed of 50mm/s and a gain of 10 mm/mV. This recorder provided digital recordings in SCP format. The acquisition process was performed by a trained nurse.

2.2. Signal Preprocessing

ECG was delineated so that QRS complexes and T waves, as well as their onset and end, were detected. This was performed by a wavelet transform delineation technique [11]. Then, baseline wander was reduced by means of cubic splines [12]. The vectorcardiogram was synthesized using the inverse Dower matrix [13].

2.3. Loop alignment and averaging

In order to attenuate noise, respiratory influence and muscular activity, depolarization and repolarization loops were first aligned with respect to a reference loop and then averaged. The reference loop is selected as the first visually checked normal loop, $\boldsymbol{Z_R}$, consisting of a $3 \times (k + 2\Delta)$ matrix containing at each row the leads X, Y and Z, respectively. Spatial and temporal alignment was performed in terms of scaling, rotation and time synchronization of the loops, as presented in [14].

Thus, three transformations were considered to perform the alignment. This process can be described as:

$$\boldsymbol{Z} = \alpha \boldsymbol{\mathcal{Q}} \boldsymbol{Z_R} \boldsymbol{J_\tau} \tag{1}$$

where $\boldsymbol{Z}$ and $\boldsymbol{Z_R}$ denote the $3 \times K$ and $3 \times (K + 2\Delta)$ matrices that contain in each row K or $K + 2\Delta$ samples corresponding to leads X,Y,Z of the loop to be aligned and the reference loop, respectively. Scaling was controlled by the positive parameter α, that allows loop expansion or contraction, whereas rotational changes of the heart were introduced by the 3×3 rotation matrix $\boldsymbol{\mathcal{Q}}$. Finally, time synchronization was described by the integer time shift τ in the shift matrix $\boldsymbol{J_\tau}$, which was defined as

$$\boldsymbol{J_\tau} = \begin{bmatrix} 0_{\Delta+\tau} \\ I \\ 0_{\Delta-\tau} \end{bmatrix}$$

where $\tau = -\Delta, ..., \Delta$, the identity matrix I is $K \times K$, and the top and bottom zero matrices are $(\Delta + \tau) \times K$ and $(\Delta - \tau) \times K$, respectively. Parameter Δ corresponds to the 2Δ additional samples that the reference loop $\boldsymbol{Z_R}$ has in order to allow for time synchronization of observations of different subsets of K samples.

The optimal estimates for α, τ and $\boldsymbol{\mathcal{Q}}$ were determined by solving the minimization problem

$$\epsilon^2_{min} = \min_{\alpha,\boldsymbol{\mathcal{Q}},\tau} \|\boldsymbol{Z} - \alpha\boldsymbol{\mathcal{Q}}\boldsymbol{Z_R}\boldsymbol{J_\tau}\|^2_F \tag{2}$$

where ϵ^2 represents the error, calculated as the Frobenius norm of the difference between the actual and the reference loop subjected to the transformations. ϵ^2 is minimized by first finding the estimates for α and $\boldsymbol{\mathcal{Q}}$ for every value of τ and then selecting the value of τ that minimizes the error. For a fully detailed explanation of the alignment process see [14].

Depolarization loops are aligned and the estimated transformations for each heartbeat are applied to align the repolarization loops. Then, depolarization and repolarization loops are averaged in order to obtain a clean and robust mean QRS and T loop. Then, the dominant vectors of the average loops, denoted by $\boldsymbol{v}_{\mathrm{QRS}}$ and $\boldsymbol{v}_{\mathrm{T}}$, are obtained by averaging the whole set of vectors that form each loop. These set of vectors describe the dominant direction of the electrical wavefront along the depolarization ($\boldsymbol{v}_{\mathrm{QRS}}$) and the repolarization ($\boldsymbol{v}_{\mathrm{T}}$) processes.

2.4. Angles estimation based on dominant vectors of depolarization and repolarization loops

We estimated the angle between the dominant vectors of depolarization and repolarization phases in the three dimensional space (θ_{RT}, the so-called spatial QRS-T angle). It is defined as the angle measured in the plane that formed by the maximum vectors of the QRS complex and the T-wave. It usually differs from the angle of the projections of the QRS and T axes in the frontal plane XY, denoted by θ_{RT-XY}, and which was also calculated in our study.

Next, we estimated the absolute angles between vectors $\boldsymbol{v}_{\mathrm{QRS}}$ and $\boldsymbol{v}_{\mathrm{T}}$ and the three orthogonal planes, $\Phi_{\mathrm{R}-\mathcal{P}}$ and $\Phi_{\mathrm{T}-\mathcal{P}}$, where $\mathcal{P} \in \{XZ, XY, YZ\}$ denotes each orthogonal plane formed by the two directions referred to $\mathcal{P}$. Finally, we also estimated the difference between them with respect to each orthogonal plane.

2.5. Loop morphology

Loop morphology was assessed by means of planarity and roundness measurements. *Planarity* is a measure of how well the VCG can be approximated by a plane or whether it is not possible, since the VCG is so curved that it is

really distributed along the 3D spatial loop. *Roundness* measurements were referred to 2D planar projections of the VCG, taking values in the range [0-1] (where 1 means that the projection is closer to a circle than to a straight line, whereas roundness close to 0 reflects the opposite and intermediate situations - an ellipsoidal shape of the VCG-) with different axes ratios as function of roundness.

If we denote the eigenvalues of the average loop matrix as $\lambda_i, i = 1, 2, 3$, sorted in descending order, the planarity of the loops is defined as

$$\rho_L = \frac{\lambda_3}{\lambda_1} \tag{3}$$

where ρ can take values between zero (entirely planar loop) and one (loop that equally extends into the three dimensions). Features will be obtained for both the depolarization and repolarization loops, being indicated by the subscript $_L$ values $_R$ or $_T$, respectively. Planarity can also be analysed by features σ_L and δ_L, which can take values in the range [0-1] (reflecting more planar loops when σ_L is close to 1 and δ is close to 0):

$$\sigma_L = \frac{\lambda_1 + \lambda_2}{\lambda_1 + \lambda_2 + \lambda_3} \tag{4}$$

$$\delta_L = \frac{\lambda_3}{\lambda_1 + \lambda_2} \tag{5}$$

QRS and T wave complexity was defined as the ratio between the second to the first eigenvalues, denoted by C:

$$C_L = \frac{\lambda_2}{\lambda_1} \tag{6}$$

The geometrical interpretation of C refers to the roundness of the loop [15]. This feature was also obtained for each plane $\mathcal{P} \in \{XZ, XY, YZ\}$, corresponding to the loop projection onto each orthogonal plane. Eigenvalues obtained on the projection were ν_1, ν_2, sorted in descending order. Thus, the roundness of the loops projected on each plane was defined as

$$\varrho_{L-\mathcal{P}} = \frac{\nu_2}{\nu_1} \tag{7}$$

2.6. Statistical analysis

A descriptive analysis including angles, planarity and characteristics was performed using mean ± standard deviation or median (interquartile range) to assess the differences between each group (Preterm-AGA and Preterm-IUGR) and controls. The results were compared by t-test or Wilcoxon-Mann-Whitney to compare means and standard deviations or medians and interquartile ranges, respectively, and χ^2 to compare percentages. Multivariate analysis by linear or quantile regression was used to adjust for age, height, gender and heart rate.

3. Results

Estimated angles and morphology measurements were obtained on the cohort of 125 subjects described in Section 2.1, who form the three groups under study: 60 controls, 32 preterm-AGA, 33 preterm-IUGR. The median and interquartile ranges of the explored parameters are shown in Tables 2 and 3, whereas perinatal and anthropometric characteristics of the study populations are shown in Table 1.

Table 1: Baseline and perinatal characteristics of the study populations. AGA (appropriate growth for gestational age), IUGR (intrauterine growth restriction). Data are mean ±standard deviation or median (interquartile range). *p<0.05 by T-test, Wilcoxon-Mann-Whitney or χ^2 as compared to controls.

	Controls n=60	Preterm AGA n=32	Preterm IUGR n=33
Birthweight (g)	3444±379.4	1872±614.7*	1162±351.9*
Gestational age at delivery (weeks)	39.5±1.3	31.6±3.1*	32.0±2.4*
Birthweight centile	56(37-81)	48(30-85)	0(0-0)*
Caucasian ethnicity (%)	95.1	93.9	80.0*
Male gender (%)	53.2	39.4	37.1
Age (years)	12.1(10.5-12.4)	10.4(8.5-11.3)*	9.41(8.3-11.4)*
Heart rate (bpm)	77.66±11.83	88.30±10.94*	81.4±9.26*
Height (cm)	148.5(137.8-154.3)	135.2(129.7-145.1)*	135(129.2-147.5)*
Weight (kg)	43.3(35.9-48.0)	32.8(28.2-41.1)*	34.4 (28.5-41.7)*
Body mass index (kg/ m^2)	19.0(17.1-20.6)	17.24(15.9-20.1)	18.1(16.4-19.6)

As expected, both preterm-IUGR and preterm-AGA cases presented lower birthweight and gestational age at delivery as compared with controls. Preterm-IUGR cases also showed a lower birthweight centile as compared with controls and preterm-AGA. The proportion of males was similar among groups, while the preterm-IUGR subgroup presented a lower prevalence of Caucasian ethnicity. Heart rate was significatively higher for preterm-AGA and preterm-IUGR, since these subjects had lower stroke volume which was compensated by increasing the heart rate [4]. Both preterm-IUGR and preterm-AGA cases showed significantly lower age, height and weight (with preserved body mass index) at evaluation as compared with controls. All subjects were asymptomatic, and none of them received medication for any cardiac condition.

Tables 2 and 3 also highlight obtained p-values lower than 0.05 by applying the Wilcoxon-Mann-Witney or the Student's t-test for the comparisons between the three different groups of subjects. We studied differences between the control group and the preterm-AGA and preterm-IUGR groups.

Figure 1 depicts the graphical comparison between the three groups (one example of each group under study, in pairs). In this Figure, a comparison of the preterm-AGA and the preterm-IUGR groups with respect to the control group was represented, whereas Figure 2 shows the comparison between the dominant vectors of the depolarization and repolarization loops for the analysis of one subject from the preterm-IUGR and another subject from the preterm-AGA. Furthermore, for the sake of clarity in graphical representation, the projections of the loops on the plane with clearer differences were represented (instead of representing them in the three-dimensional space).

In general, preterm-AGA and preterm-IUGR subjects presented larger values for angle measurement $\Phi_{\text{R-XY}}$ than controls, being also statistically significant when adjusting the data by age, height, gender and heart rate. In the particular case of preterm-IUGR, the angle difference $\Phi_{\text{R-XY}} - \Phi_{\text{T-XY}}$ was also significant, being even larger than for the preterm-AGA group.

Roundness measurements revealed significant differences between preterm-AGA and control groups, presenting the latter ones lower roundness measurements when analyzing the depolarization loops in the planes XZ and YZ.

Table 2: Vectocardiographic angle features of the study population. θ_{RT} and $\theta_{\text{RT-XY}}$ denote the so-called spatial QRS-T and frontal QRS-T angles, respectively. Absolute angles between vectors $\boldsymbol{v}_{\text{QRS}}$ or $\boldsymbol{v}_{\text{T}}$ and the three orthogonal planes of the space are denoted by $\Phi_{\text{R}-\mathcal{P}}$ and $\Phi_{\text{T}-\mathcal{P}}$, where $\mathcal{P} \in \{XZ, XY, YZ\}$ refers to each orthogonal plane. AGA (appropriate growth for gestational age), IUGR (intrauterine growth restriction). Subscripts R and T refer to the depolarization and repolarization loops, respectively. Data are mean ± standard deviation or median (interquartile range). * p-value < 0.05 by Wilcoxon-Mann-Whitney or t-test as compared to controls. † p-value < 0.05 adjusted by age, height, gender and heart rate, controls as reference category.

	Controls n=60	Preterm AGA n=32	Preterm IUGR n=33
θ_{RT}	15.28(8.390-24.10)	10.63(5.539-20.76)	16.58(6.890-22.73)
$\theta_{\text{RT-XY}}$	6.57(2.72-11.31)	4.68(2.20-12.89)†	6.52(3.88-15.82)
$\Phi_{\text{R-XZ}}$	37.60(29.91-40.82)	32.64(28.90-36.78)*	34.24(28.58-39.91)
$\Phi_{\text{R-XY}}$	20.03(10.11-28.64)	27.77(16.59-33.23)*	25.48(19.79-33.56)*†
$\Phi_{\text{R-YZ}}$	45.95±9.31	45.85±9.02	43.06±8.92
$\Phi_{\text{T-XZ}}$	36.42(32.05-38.83)	31.89(29.07-38.14)	32.01(28.58-38.63)†
$\Phi_{\text{T-XY}}$	29.39(13.71-27.26)	23.59(17.63-26.80)	21.52(12.77-25.89)
$\Phi_{\text{T-YZ}}$	47.24(38.75-52.86)	46.57(41.63-53.30)	47.86(41.16-56.55)
$\Phi_{\text{R-XZ}} - \Phi_{\text{T-XZ}}$	1.70(-3.97-5.43)	-0.52(-6.01-4.69)	0.88(2.33-6.10)
$\Phi_{\text{R-XY}} - \Phi_{\text{T-XY}}$	-0.491±14.15	3.001±12.99	5.279±12.15*†
$\Phi_{\text{R-YZ}} - \Phi_{\text{T-YZ}}$	-0.662±12.50	-1.752±10.67	-4.854±12.74

Table 3: Vectocardiographic loops morphology of the study population. ρ_{L}, σ_{L}, and δ_{L} denote measures of planarity of loop L. C_{L} and $\varrho_{\mathrm{L}-\mathcal{P}}$ refer to roundness measurements. $\mathcal{P} \in \{XZ, XY, YZ\}$ refers to the projection of the loop in each orthogonal plane $\mathcal{P}$, whereas the subscript L will be replaced by R or T, depending on whether it refers to the depolarization or repolarization loops. AGA (appropriate growth for gestational age), IUGR (intrauterine growth restriction). Subscripts R and T refer to the depolarization and repolarization loops, respectively. Data are median (interquartile range). * p-value < 0.05 by Wilcoxon-Mann-Whitney or t-test as compared to controls. † p-value < 0.05 adjusted by age, height, gender and heart rate, controls as reference category.

	Controls n=60	Preterm AGA n=32	Preterm IUGR n=33
ρ_{R}	0.044(0.029-0.067)	0.036(0.022-0.058)	0.037(0.022-0.051)
ρ_{T}	0.031(0.021-0.054)	0.037(0.028-0.061)	0.034(0.021-0.048)
σ_{R}	0.967(0.953-0.979)	0.975(0.956-0.982)	0.971(0.961-0.982)
σ_{T}	0.973(0.955-0.981)	0.968(0.946-0.976)	0.972(0.955-0.981)
δ_{R}	0.033(0.022-0.045)	0.024(0.017-0.046)	0.028(0.017-0.040)
δ_{T}	0.028(0.019-0.044)	0.031(0.024-0.054)	0.027(0.019-0.044)
C_{R}	0.316(0.222-0.423)	0.264(0.171-0.331)	0.291(0.202-0.420)
C_{T}	0.135(0.103-0.189)	0.149(0.123-0.192)	0.134(0.096-0.189)
$\varrho_{\mathrm{R\text{-}XZ}}$	0.384(0.257-0.489)	0.291(0.194-0.396)*†	0.335(0.247-0.516)
$\varrho_{\mathrm{R\text{-}XY}}$	0.113(0.066-0.162)	0.086(0.049-0.155)†	0.117(0.074-0.187)
$\varrho_{\mathrm{R\text{-}YZ}}$	0.330(0.211-0.452)	0.227(0.164-0.331)*†	0.276(0.212-0.346)
$\varrho_{\mathrm{T\text{-}XZ}}$	0.157(0.124-0.198)	0.166(0.113-0.204)	0.141(0.102-0.235)
$\varrho_{\mathrm{T\text{-}XY}}$	0.054(0.037-0.067)	0.072(0.042-0.110)*	0.054(0.032-0.095)
$\varrho_{\mathrm{T\text{-}YZ}}$	0.201(0.151-0.272)	0.155(0.111-0.235)*	0.171(0.134-0.281)

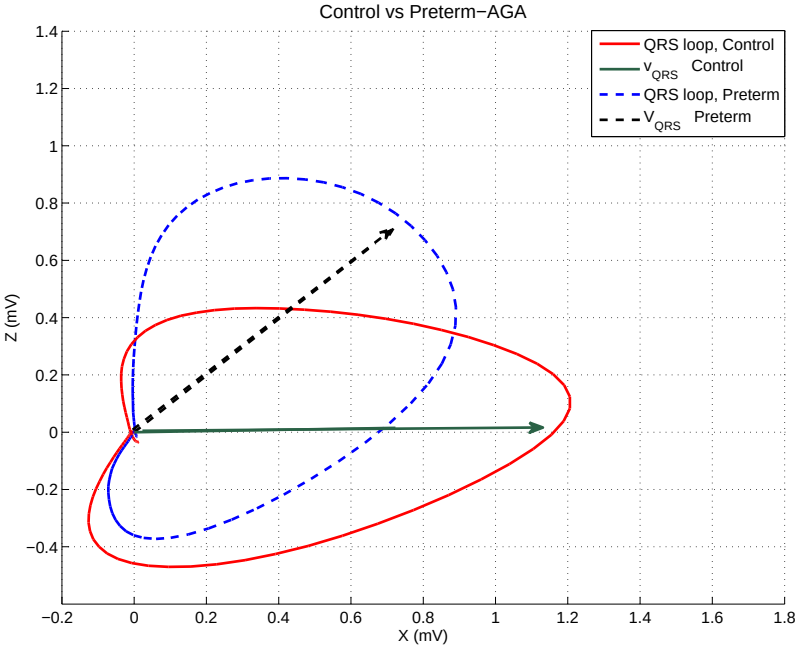

(a)

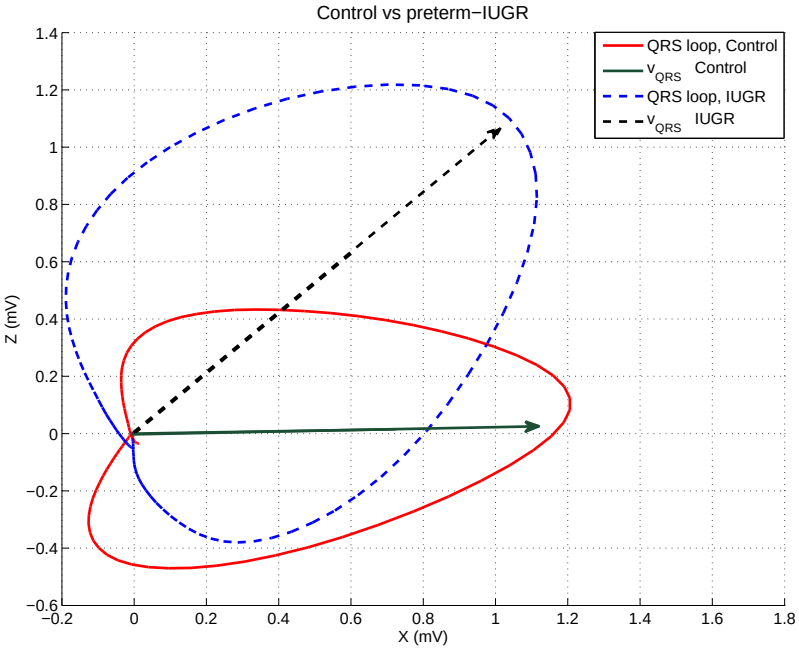

(b)

Figure 1: Average of all depolarization loops for a patient and their corresponding dominant vectors ($\boldsymbol{v}_{\mathrm{QRS}}$) projected onto the XZ-plane. (a) Subject of the control group vs. a subject from the preterm group. (b) Same subject of the control group vs. a subject from the IUGR group.

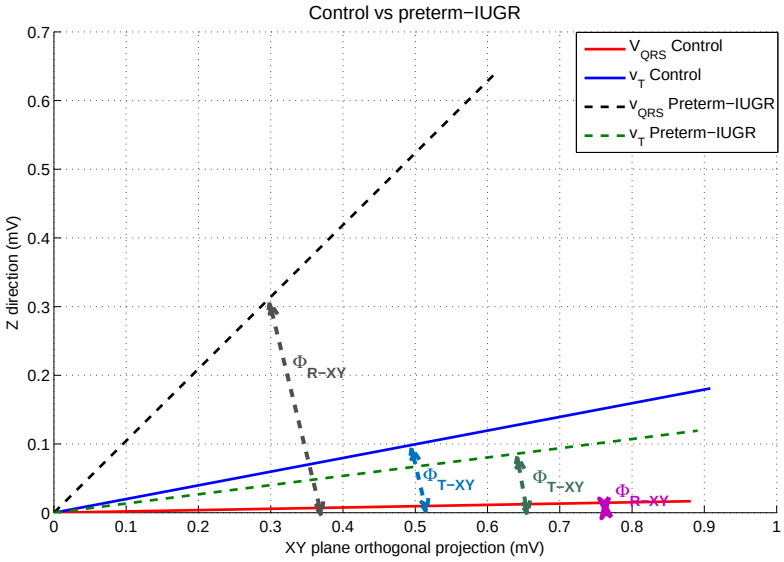

(a)

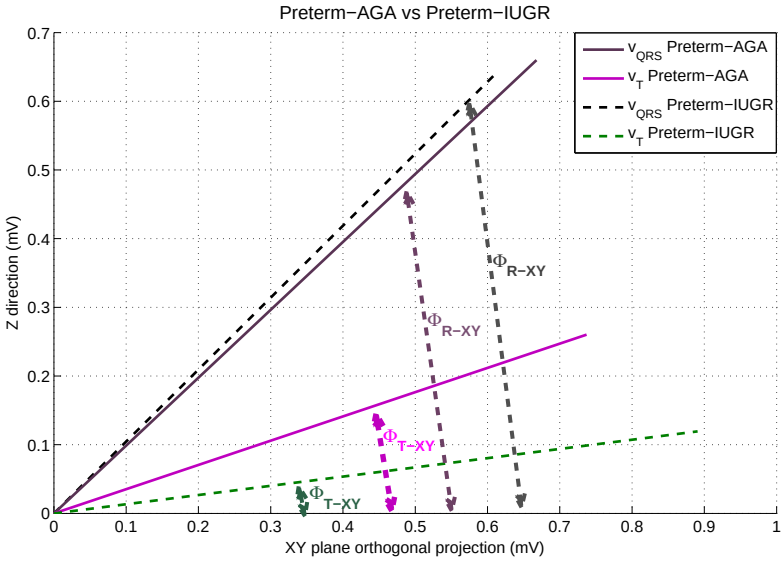

(b)

Figure 2: (a) Projection of dominant vectors of the average depolarization and repolarization loops on XY plane (and the respective absolute angles) for a subject of the control group and a subject from the preterm-IUGR group. (b) Projection of dominant vectors of the average depolarization and repolarization loops on XY plane (and the respective absolute angles) for a subject of the preterm-AGA group and a subject from the preterm-IUGR group.

4. Discussion of results

This paper reports for the first time significant changes in depolarization-repolarization angles and VCG loop morphology in IUGR and preterm individuals, respectively. These findings support the notion of electrophysiological remodeling in both IUGR and prematurity, and could partially explain the higher cardiovascular morbidity previously reported in these populations.

This study has included a group of preadolescents who suffered severe IUGR in uterus that lead to medically induced preterm delivery. This preterm-IUGR group was characterized by a wider QRS-T angle (θ_{RT}) in relation to body plane, with no significant differences in roundness and planarity. While a non-significant trend to higher values of spatial (θ_{RT}) and frontal ($\theta_{\mathrm{RT\text{-}XY}}$) QRS-T angles was observed, significantly higher angles in the frontal plane (XY) could be demonstrated with respect to controls (Table 2). Despite being wider than in controls, their angle values were within the normal limits [16]. Usually, a wider QRS-T angle is derived by changes in T-wave axis, which has been reported to be a risk factor for cardiac events [17, 18]. However, in our study wider QRS-T angle in the XY plane was mainly due to changes in QRS axis (although there were also changes in the T-wave -significant for XZ plane, but not significant for XY frontal plane-), suggesting more significant depolarization rather than repolarization abnormalities. Wider spatial QRS-T angle has been proven to be a powerful predictor of cardiovascular mortality in general population [19, 20, 17] and of sudden arrhythmic death in survivors of acute myocardial infarction [21]. It has been also described in smokers, myocardial hypertrophy, diabetes, and high blood pressure [22]. Regarding electrical remodeling, our results are in line with previous reports suggesting lower acceleration and deceleration capacity in very preterm-IUGR fetuses [23, 24] and higher QT and JT dispersion [25] in IUGR fetuses and newborns. The electrical findings are also consistent with previous echocardiographic studies in IUGR demonstrating significant changes in the cardiac structure and function of these individuals in uterus but also in postnatal age [4]. Additional results included in the Supplementary data section showed significant correlations between left ventricular mass and depolarization-repolarization angles for preterm IUGR subjects. This can be related to the fact that severe IUGR cases typically show more spherical hearts with impaired relaxation and longitudinal motion together with a decrease in stroke volume which is compensated by an increase in heart rate in order to maintain cardiac output [26, 27]. These car-

diac changes are thought to be a response to the placental insufficiency which is usually associated with fetal hypoxia, undernutrition and pressure/volume overload [28]. We speculate that the link between our electrical results and the previously reported structural changes could be explained by the location of the Purkinje system inside the endocardium. The pressure overload and hypoxia -usually associated with IUGR- is known to mostly affect the endocardial fibers leading to a decreased longitudinal motion and could also predominantly affect the endocardial Purkinje system and change the vector gradient of depolarization and repolarization. It is also shown that this pressure overload mainly affects the basal part of the ventricle which might contribute to the heterogeneity in the distribution of the endocardial pressure, explaining wider angles as the T- vectors might not be in the same direction as the QRS ones [22].

The present study also included a group of normally grown cases who were spontaneously born preterm. This preterm-AGA group was characterized by a reduced frontal QRS-T angle and roundness with preserved planarity. Similar results in the QRS-T angle were reported in healthy middled-age subjects with a genetic polymorphism of the KCNH2(HERG), a gene with functional electrical properties. Smaller values in the QRS-T angle could reflect a desynchronization between repolarization and depolarization that could be associated with increased cardiovascular mortality(7). However, it has been suggested that frontal QRS-T angle turned out to be a bad substitute for spatial QRS-T angle [29, 16]. Therefore, this result needs to be carefully interpreted. The less round projections of the VCG observed in preterm-AGA could also be associated with higher cardiovascular risk. The electrical changes observed in preterm-AGA are consistent with a previous study suggesting longer QT interval, higher QT dispersion and shorter PR interval in young adults born preterm [30]. We speculate that these electrical findings could be related to the cardiac structural changes previously described in individuals born prematurely. Adults born preterm show smaller and shorter hearts with increased left ventricular mass and impaired longitudinal motion [5]. This cardiovascular remodelling seems to be an adaptive response to the relative pressure overload that the immature cardiovascular system suffers during the neonatal period after a premature delivery [31], though inflammation, infection or other pathophysiological mechanisms potentially associated with spontaneous preterm delivery could also explain the cardiac response observed in these individuals. The different pathophysiological mechanisms observed in IUGR and spontaneous preterm delivery could

determine the distinct pattern of electrical remodelling observed in preterm-AGA and preterm-IUGR in our study.

Strengths and limitations of the present deserve further comments. Our work is pioneer in establishing the electrophysiological consequences of prematurity and IUGR by VCG. The study populations were well-defined and phenotyped from fetal life, permitting a clear distinction between spontaneous and medically-induced preterm delivery, which are usually mixed up in the literature. IUGR cases were also carefully selected including umbilical artery Doppler in the definition, which is an excellent surrogate of severe placental insufficiency. In addition, the VCG measurements used here are less susceptible to noise and definition problems as compared to the conventional ECG analysis including QT dispersion. Despite these strengths, we acknowledge potential limitations. Firstly, the relatively limited sample size might have prevented demonstrating significant differences in some angular measurements and planarity. Secondly, we acknowledge that differences in age at evaluation between cases and controls might have influenced the results. Thirdly, potential confounding variables such as smoking, mental stress or family history were not included in the analysis. Fourthly, the study was performed in preadolescent age which warrants future studies to evaluate the persistence of these findings in older ages and its potential association with cardiovascular adverse events. Additionally, while VCG analysis based on the ECG is a non-invasive low-cost approach that has been shown to be useful for risk assessment, it is still not widely used in clinical practice. Finally, future studies are warranted to better determine the mechanisms underlying the electrical changes observed in these populations.

5. Conclusions

Our study demonstrates for the first time particular patterns of electrical remodeling associated with both prematurity and IUGR. Significantly wider angles between the depolarization dominant vector and the frontal XY body plane were observed for preterm-IUGR subjects, resulting in significantly wider angles between depolarization and repolarization vectors. Significantly lower angles were observed for the repolarization vector and the XZ plane in preterm-IUGR subjects with respect to controls. The classical frontal QRS-T angle was significantly narrower in preadolescents who were spontaneously born preterm with respect to controls. Moreover, significantly less roundness

measurements for the depolarization loop projections in all three orthogonal planes were also observed.

These findings might be related to the previously described cardiac structural changes and increased cardiovascular risk in these populations. Future studies are warranted to confirm these results and further describe the electrical characteristics of these individuals and its potential long-term consequences.

Acknowledgements

N. Ortigosa acknowledges the support from Generalitat Valenciana under grants PrometeoII/2013/013, ACOMP/2015/186, and MINECO under grant MTM2013-43540-P.

This project has also been partially funded by TEC2013-42140-R and TIN2014-53567-R from CICYT, by Grupo Consolidado BSICoS from DGA (Aragón) and European Social Fund, the Erasmus + Programme of the European Union (Framework Agreement number: 2013-0040), the South-Eastern Norway Regional Health Authority, the Bergesen foundation and grants from Instituto de Salud Carlos III (grant numbers PI12/00801 and PI14/00226), Ministerio de Economía y Competitividad (grant number SAF2012-37196), cofinanced by the Fondo Europeo de Desarrollo Regional de la Unión Europea "Una manera de hacer Europa", Fundación Mutua Madrileña, Obra Social La Caixa (Spain), Cerebra Foundation for the Brain Injured Child (Carmarthen, Wales, UK), and the European Commission (VP2HF no.611823). This publication reflects the views only of the authors, and the Commission cannot be held responsible for any use which may be made of the information contained therein. The computation was performed by the ICTS 0707NAN-BIOSIS, by the High Performance Computing Unit of the CIBER in Bioengineering, Biomaterials & Nanomedicine (CIBER-BBN) at the University of Zaragoza.

References

[1] Barker DJ. The fetal and infant origins of adult disease. BMJ. 1990;301(6761):1111.

[2] Figueras F, Gratacos E. Update on the diagnosis and classification of fetal growth restriction and proposal of a stage-based management protocol. Fetal Diagn Ther. 2014;36(2):86–98.

[3] Crispi F, Hernandez-Andrade E, Pelsers MM, Plasencia W, Benavides-Serralde JA, Eixarch E, et al. Cardiac dysfunction and cell damage across clinical stages of severity in growth-restricted fetuses. Am J Obstet Gynecol. 2008;199(254):e1–e8.

[4] Crispi F, Bijnens B, Figueras F, Bartrons J, Eixarch E, Noble FL, et al. Fetal growth restriction results in remodeled and less efficient hearts in children. Circulation. 2010;121(22):2427–2436.

[5] Lewandowski AJ, Augustine D, Lamata P, Davis EF, Lazdam M, Francis J, et al. Preterm heart in adult life: cardiovascular magnetic resonance reveals distinct differences in left ventricular mass, geometry, and function. Circulation. 2013;127(2):197–206.

[6] Cirillo PM, Cohn BA. Pregnancy Complications and Cardiovascular Disease Death: 50-Year Follow-Up of the Child Health and Development Studies Pregnancy Cohort. Circulation. 2015;132(13):1234–1242.

[7] Blair PS, Platt MW, Smith IJ, Fleming PJ. Sudden infant death syndrome and sleeping position in pre-term and low birth weight infants: an opportunity for targeted intervention. Arch Dis Child. 2006;91(2):101–106.

[8] Baird TM. Clinical correlates, natural history and outcome of neonatal apnoea. Semin Neonatol. 2004;9(3):205–211.

[9] Cutler MJ, Jeyaraj D, Rosenbaum DS. Cardiac electrical remodeling in health and disease. Trends Pharmacol Sci. 2011;32(3):174–180.

[10] Figueras F, Meler E, Iraola A, Eixarch E, Coll O, Figueras J, et al. Customized birthweight standards for a Spanish population. Eur J Obstet Gynecol Reprod Biol. 2008;136:20–24.

[11] Martínez JP, Almeida R, Olmos S, Rocha AP, Laguna P. A Wavelet-Based ECG Delineator: Evaluation on Standard Databases. IEEE Trans Biomed Eng. 2004;51(4):570–581.

[12] Meyer CR, Keiser HN. Electrocardiogram baseline noise estimation and removal using cubic splines and state-space computation techniques. Comput Biomed Res. 1977;10:459–470.

[13] Edenbrandt L, Pahlm O. Vectorcardiogram synthetized from a 12-lead ECG: Superiority of the inverse Dower matrix. J Electrocardiol. 1988;21:361–367.

[14] Sörnmo L. Vectorcardiographic loop alignment and morphologic beat-to-beat. IEEE Trans Biomed Eng. 1998;45:1401–1413.

[15] Laguna P, Martinez JP, Pueyo E. Techniques for ventricular repolarization instability assessment from the ECG. Proceedings of the IEEE. 2016;DOI:10.1109/JPROC.2015.2500501.

[16] Macfarlane PW. The frontal plane QRS-T angle. Europace. 2012;14(6):773–775.

[17] Rautaharju PM, Nelson JC, Kronmal RA, Zhang ZM, Robbins J, Gottdiener JS, et al. Usefulness of T-axis deviation as an independent risk indicator for incident cardiac events in older men and women free from coronary heart disease (the Cardiovascular Health Study). Am J Cardiol. 2001;88:118–123.

[18] Kors JA, de Bruyne MC, Hoes AW, van Herpen G, Hofman A, van Bemmel JH, et al. T axis as an indicator of risk of cardiac events in elderly people. Lancet. 1998;352:601–605.

[19] Kardys I, Kors JA, van der Meer IM, Hofman A, van der Kuip DA, Witteman JC. Spatial QRS-T angle predicts cardiac death in a general population. Eur Heart J. 2003;24:1357–1364.

[20] Yamazaki T, Froelicher VF, Myers J, Chun S, Wang P. Spatial QRS-T angle predicts cardiac death in a clinical population. Heart Rhythm. 2005;2(1):73–78.

[21] Malik M, Hnatkova K, Batchvarov VN. Post infarction risk stratification using the 3-D angle between QRS complex and T-wave vectors. J Electrocardiol. 2004;37:S201–208.

[22] Voulgari C, Pagoni S, Tesfaye S, Tentolouris N. The spatial QRS-T angle: implications in clinical practice. Curr Cardiol Rev. 2013;9(3):197–210.

[23] Stampalija T, Casati D, Monasta L, Sassi R, Rivolta MW, Muggiasca ML, et al. Brain sparing effect in growth-restricted fetuses is associated with decreased cardiac acceleration and deceleration capacities: a case-control study. BJOG. 2015;DOI: 10.1111/1471-0528.13607.

[24] Stampalija T, Casati D, Montico M, Sassi R, Rivolta MW, Maggi V, et al. Parameters influence on acceleration and deceleration capacity based on trans-abdominal ECG in early fetal growth restriction at different gestational age epochs. Eur J Obstet Gynecol Reprod Biol. 2015;188:104–112.

[25] Fouzas S, Karatza AA, Davlouros PA, Chrysis D, Alexopoulos D, Mantagos S, et al. Heterogeneity of ventricular repolarization in newborns with intrauterine growth restriction. Early Hum Dev. 2014;90(12):857–862.

[26] Cruz-Lemini M, Crispi F, Valenzuela-Alcaraz B, Figueras F, Sitges M, Bijnens B, et al. Fetal cardiovascular remodelling persists at 6 months of life in infants with intrauterine growth restriction. Ultrasound Obstet Gynecol. 2015;DOI: 10.1002/uog.15767.

[27] Cruz-Lemini M, Crispi F, Valenzuela-Alcaraz B, Figueras F, Gomez O, Sitges M, et al. A fetal cardiovascular score to predict infant hypertension and arterial remodeling in intrauterine growth restriction. Am J Obstet Gynecol. 2014;210(6):e1–e22.

[28] Crispi F, Bijnens B, Sepulveda-Swatson E, Cruz-Lemini M, Rojas-Benavente J, Gonzalez-Tendero A, et al. Postsystolic shortening by myocardial deformation imaging as a sign of cardiac adaptation to pressure overload in fetal growth restriction. Circ Cardiovasc Imaging. 2014;7(5):781–787.

[29] Rautaharju PM, Prineas RJ, Zhang ZM. A simple procedure for estimation of the spatial QRS/T angle from the standard 12-lead electrocardiogram. J Electrocardiol. 2007;40(3):300–304.

[30] Bassareo PP, Fanos V, Puddu M, Cadeddu C, Balzarini M, Mercuro G. Significant QT interval prolongation and long QT in young adult ex-preterm newborns with extremely low birth weight. J Matern Fetal Neonatal Med. 2011;24(9):1115–1118.

436 [31] Lewandowski AJ, Leeson P. Preeclampsia, prematurity and cardiovas-
437 cular health in adult life. Early Hum Dev. 2014;90(11):725–729.

Supplementary material

Supplemental methods

Each individual underwent a comprehensive M-mode and 2D echocardiography using a commercially available ultrasound scanner (Vivid E9, General Electric Healthcare) just after ECG acquisition. Echocardiographic images were analyzed offline with commercially available software (EchoPac, General Electric Healthcare, version 108.1.6) by an experienced observer. Left ventricular end-diastolic wall thicknesses were measured by M-mode from a parasternal long-axis view. Cardiac diameters were determined from 2D images from an apical 4-chamber view at end-diastole. Left ventricular mass was then computed using the ASE formula [1]. Pearson test was performed in order to evaluate the correlation between the left ventricular mass and vectorcardiographic parameters. In order to visualize the covariance between them, observed and linear predicted values were plotted by groups.

Supplemental results

Pearson correlation results between left ventricular mass and vectorcardiographic parameters are displayed in Table 1. Left ventricular mass showed a significant correlation with $\Phi_{\text{T-YZ}}$, ρ_{T}, δ_{T}, C_{T}, σ_{T}, $\varrho_{\text{T-XZ}}$ and $\varrho_{\text{T-XY}}$ among preterm AGA individuals. It also showed a significant correlation with θ_{RT}, $\theta_{\text{RT-XY}}$, $\Phi_{\text{R-XZ}}$, $\Phi_{\text{R-XY}}$, $\Phi_{\text{R-XZ}} - \Phi_{\text{T-XZ}}$, , $\Phi_{\text{R-XY}} - \Phi_{\text{T-XY}}$, ρ_{R}, δ_{R} and σ_{R} among preterm IUGR cases.

References

[1] Lang RM, Badano LP, et al VMA. Recommendations for cardiac chamber quantification by echocardiography in adults: an update from the American Society of Echocardiography and the European Association of Cardiovascular Imaging. J Am Soc Echocardiogr. 2015;28(1):1–39 e14.

Table 1: Pearson correlation values between left ventricular mass and vectorcardiographic (angle features and loops morphology) characteristics within preterm AGA and preterm IUGR populations. *p<0.05 from Pearson test

	Preterm AGA n=32	Preterm IUGR n=33
Angle features		
θ_{RT}	0.1846	0.4668*
$\theta_{\text{RT-XY}}$	0.0892	0.5391*
$\Phi_{\text{R-XZ}}$	-0.3369	-0.4253*
$\Phi_{\text{R-XY}}$	-0.1430	0.4883*
$\Phi_{\text{R-YZ}}$	0.3202	-0.0963
$\Phi_{\text{T-XZ}}$	-0.2581	0.3455*
$\Phi_{\text{T-XY}}$	-0.2175	-0.2182
$\Phi_{\text{T-YZ}}$	0.3563*	-0.2182
$\Phi_{\text{R-XZ}} - \Phi_{\text{T-XZ}}$	0.0507	-0.5176*
$\Phi_{\text{R-XY}} - \Phi_{\text{T-XY}}$	0.0248	0.5071*
$\Phi_{\text{R-YZ}} - \Phi_{\text{T-YZ}}$	-0.0464	0.1211
Loops morphology		
ρ_{R}	-0.0347	-0.3929*
ρ_{T}	0.4823*	0.1550
σ_{R}	0.0540	0.4452*
σ_{T}	-0.3611*	-0.1478
δ_{R}	-0.0475	-0.4509*
δ_{T}	0.3692*	0.1471
C_{R}	-0.0978	0.1603
C_{T}	0.5517*	0.1468
$\varrho_{\text{R-XZ}}$	-0.1497	0.0942
$\varrho_{\text{R-XY}}$	-0.1150	0.0449
$\varrho_{\text{R-YZ}}$	0.0370	0.2837
$\varrho_{\text{T-XZ}}$	0.4528*	0.1258
$\varrho_{\text{T-XY}}$	0.5193*	0.2609
$\varrho_{\text{T-YZ}}$	0.3166	0.0651

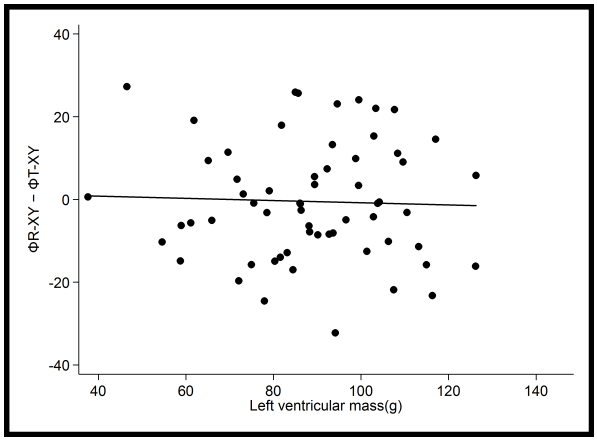

(a)

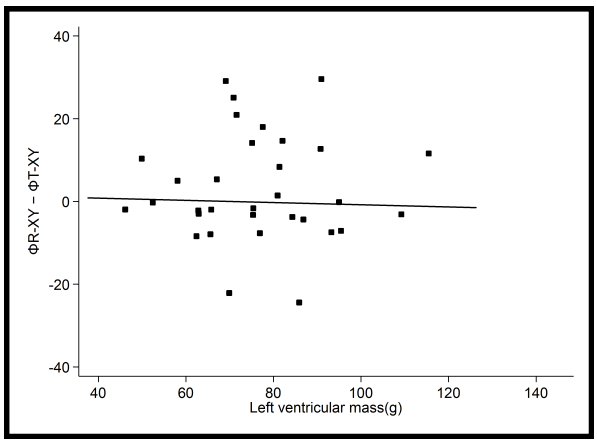

(b)

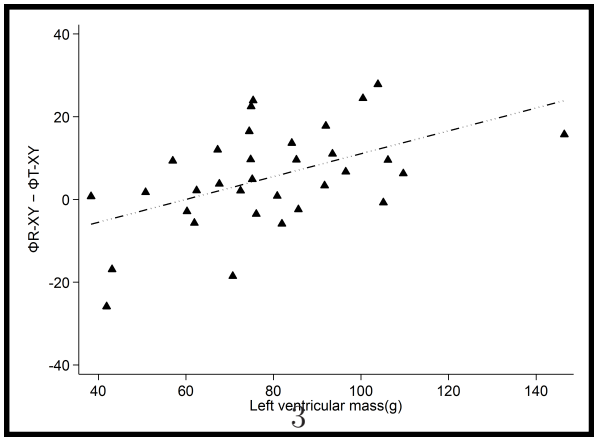

(c)

Figure 1: Relation between left ventricular mass and the difference between R and T wave projections into XY plane for a)Controls, b)Preterm AGA, c)Preterm IUGR.